Astronomy & Astrophysics

A complete ^{12}CO 2−1 map of M 51 with HERA

I. Radial averages of CO, H I, and radio continuum

K. F. Schuster[1], C. Kramer[2], M. Hitschfeld[2], S. Garcia-Burillo[3], and B. Mookerjea[2,4]

[1] IRAM, 300 rue de la Piscine, 38406 St. Martin d'Hères, France
e-mail: schuster@iram.es
[2] KOSMA, I. Physikalisches Institut, Universität zu Köln, Zülpicher Straße 77, 50937 Köln, Germany
[3] Centro Astronomico de Yebes, IGN, 19080 Guadalajara, Spain
[4] Department of Astronomy, University of Maryland, College Park, MD 20742, USA

ABSTRACT

Context. The mechanisms governing the star formation rate in spiral galaxies are not yet clear. The nearby, almost face-on, and interacting galaxy M 51 offers an excellent opportunity to study at high spatial resolutions the local star formation laws.

Aims. In this first paper, we investigate the correlation of H_2, H I, and total gas surface densities with the star forming activity, derived from the radio continuum (RC), along radial averages out to radii of 12 kpc.

Methods. We have created a complete map of M 51 in ^{12}CO 2−1 at a resolution of 450 pc using HERA at the IRAM-30 m telescope. These data are combined with maps of H I and the radio-continuum at 20 cm wavelength. The latter is used to estimate the star formation rate (SFR), thus allowing to study the star formation efficiency and the local Schmidt law $\Sigma_{\mathrm{SFR}} \propto \Sigma_{\mathrm{gas}}^n$. The velocity dispersion from CO is used to study the critical surface density and the gravitational stability of the disk.

Results. The total mass of molecular material derived from the integrated ^{12}CO 2−1 intensities is $2 \times 10^9\ M_\odot$. The 3σ detection limit corresponds to a mass of $1.7 \times 10^5\ M_\odot$. The global star formation rate is $2.56\ M_\odot\ \mathrm{yr}^{-1}$ and the global gas depletion time is 0.8 Gyr. H I and RC emission are found to peak on the concave, downstream side of the outer south-western CO arm, outside the corotation radius. The total gas surface density Σ_{gas} drops by a factor of ~20 from $70\ M_\odot\ \mathrm{pc}^{-2}$ at the center to $3\ M_\odot\ \mathrm{pc}^{-2}$ in the outskirts at radii of 12 kpc. The fraction of atomic gas gradually increases with radius. The ratio of H I over H_2 surface densities, $\Sigma_{\mathrm{HI}}/\Sigma_{\mathrm{H2}}$, increases from ~0.1 near the center to ~20 in the outskirts without following a simple power-law. Σ_{HI} starts to exceed Σ_{H2} at a radius of ~4 kpc. The star formation rate per unit area drops from ~$400\ M_\odot\ \mathrm{pc}^{-2}\ \mathrm{Gyr}^{-1}$ in the starburst center to ~$2\ M_\odot\ \mathrm{pc}^{-2}\ \mathrm{Gyr}^{-1}$ in the outskirts. The gas depletion time varies between 0.1 Gyr in the center and 1 Gyr in the outskirts, and is shorter than in other non-interacting normal galaxies. Neither the H I surface densities nor the H_2 surface densities show a simple power-law dependence on the star formation rate per unit area. In contrast, Σ_{gas} and Σ_{SFR} are well characterized by a local Schmidt law with a power-law index of $n = 1.4 \pm 0.6$. The index equals the global Schmidt law derived from disk-averaged values of Σ_{gas} and Σ_{SFR} of large samples of normal and starburst galaxies. The critical gas velocity dispersions needed to stabilize the gas against gravitational collapse in the differentially rotating disk of M 51 using the Toomre criterion, vary with radius between 1.7 and $6.8\ \mathrm{km\ s}^{-1}$. Observed radially averaged dispersions derived from the CO data vary between $28\ \mathrm{km\ s}^{-1}$ in the center and ~$8\ \mathrm{km\ s}^{-1}$ at radii of 7 to 9 kpc. They exceed the critical dispersions by factors Q_{gas} of 1 to 5. We speculate that the gravitational potential of stars leads to a critically stable disk.

Key words. galaxies: evolution – galaxies: individual: M 51 – galaxies: ISM – galaxies: spiral – galaxies: structure

1. Introduction

M 51 is an interacting, grand-design spiral galaxy at a distance of only 8.4 Mpc seen nearly face-on (Table 1). It is rich in molecular gas, most of which is found in the two very prominent spiral arms which are presumably caused by the tidal interaction (Tully 1974b; Howard & Byrd 1990). Kinematic studies reveal unusually large streaming motions implying a strong density wave and the presence of galactic shocks (Aalto et al. 1999). The [C II] map of Nikola et al. (2001) shows two secondary lobes of emission to the northeast and southwest near the corotation radius of the density wave pattern, presumably due to cloud-cloud collisions, stimulating star formation. Calzetti et al. (2005) combine Spitzer infrared data of the Infrared Array Camera (IRAC) and the Multi Imaging Photometer for Spitzer (MIPS) with UV data from the Galaxy Evolution Explorer (GALEX). These data are used to discuss the various tracers of star formation in M 51. Enhanced star formation activity at the two lobes

seen in [C II] is probably triggered by the interaction (Nikola et al. 2001). This is also indicated by disk simulations of Toomre & Toomre (1972) which show tidal tails emerging from the disk at the positions of enhanced star formation. VLA observations of the H I line show a prominent tail outside the main disk extending to the south and east, and covering more than 25′, i.e. 100 kpc, in projected distance (Rots et al. 1990) (cf. Tilanus & Allen 1991). Meijerink et al. (2005) find that a major fraction of cold dust emission at 850 μm stems from an extended exponential disk with a scale height of 5.45 kpc, possibly also tracing total gas column densities. The kinematics of Hα emission of M 51 were recently studied by the SINGS team (Daigle et al. 2006), improving on the work of Tilanus & Allen (1991).

Its proximity and inclination make M 51 an ideal target to study the efficiency at which it forms stars from the gas under the influence of the interaction, and to compare with the star formation laws commonly found in spiral galaxies. Spiral galaxies

Table 1. Basic properties of M 51.

	M 51
RA(2000)	13:29:52.7
Dec(2000)	47:11:43
Type	SA(s)bc pec[a]
Distance [Mpc]	8.4[b]
11″ correspond to	448 pc
Heliocentric velocity [km s^{-1}]	463[a]
Position Angle [deg]	170[c]
Inclination [deg]	20[c]

References: [a] RC3 catalogue de Vaucouleurs et al. (1991), [b] Feldmeier et al. (1997), note that Takats & Vinko (2006) recently reported a distance of only 7.1 ± 1.2 Mpc, [c] Tully (1974a).

often follow two empirical laws: as star formation is fueled by the interstellar gas reservoir, the star formation rate (SFR) is proportional to a power of the total gas surface density: $\Sigma_{SFR} \propto \Sigma_{gas}^n$. This appears to hold globally when Σ_{gas} and Σ_{SFR} are averaged over the entire star-forming region of a galaxy (Schmidt 1959; Kennicutt 1998, and others) with $n = 1.4$. This may be understood assuming that Σ_{SFR} is proportional to the gas surface density over the free-fall time τ_{ff} and that the free-fall time and the gas surface density are simple functions of the average gas density ρ: $\tau_{ff} \propto \rho^{-1/2}$ and $\Sigma_{gas} \propto \rho$. This simple model leads directly to the Schmidt law with an index of 1.5 (e.g. Elmegreen 1994). More recent studies show that the global Schmidt law also appears to hold locally in individual spiral galaxies when studying radially averaged profiles of Σ_{gas} and Σ_{SFR} (Wong & Blitz 2002; Boissier et al. 2003). The second law is that the total gas surface density is of the order of a critical gas surface density given by the Toomre (1964) criterion for gravitational stability (Martin & Kennicutt 2001; Li et al. 2006).

The relative importance of the different components of the interstellar medium was addressed by Nikola et al. (2001) when trying to explain the mapped [C II] emission. In a recent study comprising all major cooling lines of the molecular gas, i.e. those of [C II], [O I], CO, and [C I], at selected spiral arm positions and the center of M 51, Kramer et al. (2005) conclude that the bulk of the emission stems from clumpy photon dominated regions. Only about 15−30% of the [C II] emission stems from dense H II regions. The [C I] and CO emission of the center region have also been studied by Israel et al. (2006); Israel & Baas (2002); Gerin & Phillips (2000). Schinnerer et al. (2004) mapped two distinct regions in the spiral arms of M 51 in HCN, HCO$^+$ and other tracers of the chemistry.

Rydbeck et al. (2004) presented a large CO 1−0 map of M 51 obtained at the Onsala-20m telescope. The inner region of M 51 were previously mapped in CO 1−0 with the FCRAO-14 m, IRAM-30 m, and NRO-45 m telescopes by Scoville & Young (1983); Lord & Young (1990); Garcia-Burillo et al. (1993b); Nakai et al. (1994); Kuno et al. (1995); Kuno & Nakai (1997). These single-dish observations reveal the large-scale emission for which interferometric observations are not sensitive. OVRO was used to create CO 1−0 maps by Rand & Kulkarni (1990) and Aalto et al. (1999). Helfer et al. (2003) used BIMA in combination with NRAO-12 m single-dish data to map the inner part of M 51 in CO 1−0.

Here, we present a complete IRAM-30 m CO 2−1 map of M 51, improving on the previous data of Garcia-Burillo et al. (1993b,a).

2. Observations

Observations of the ^{12}CO 2−1 emission from M 51 were conducted with the IRAM-30 m telescope in February 2005 using the 18 element focal plane heterodyne receiver array HERA (Schuster et al. 2004) together with the WILMA autocorrelator backend. WILMA has a channel spacing of 2.6 km s^{-1} (2 MHz) and a bandwidth of 1200 km s^{-1} (930 MHz). Pixel 2 of the second HERA polarization showed excess noise and was ignored from further analysis.

Observations were conducted in position switched on-the-fly (OTF) mode scanning M 51 in right ascension. Sampling was 6″ in RA. HERA was rotated by 18.5° to obtain a spacing of 7.6″ in declination between adjacent scan lines (Schuster et al. 2004). This corresponds to near Nyquist sampling for a half power beamwidth (*HPBW*) of 11″. The resulting map has a size of 11′ × 11′. Figure 1 shows the 7′ × 10′ sub-region where CO was detected. An emission-free reference position was selected at offsets (10′, 0′). The mean baseline rms is 18 mK at 5 km s^{-1} velocity resolution on the T_A^* scale. To correct to first order for the telescope efficiencies, i.e. to go from the T_A^* scale to the T_{mb} scale, we simply multiplied the antenna temperature data with the ratio of forward efficiency $F_{eff} = 0.91$ over main beam efficiency $B_{eff} = 0.52$. These numbers show that the mapped spatial structure of M 51 is to some extent smeared out by the error beams of the IRAM-30 m telescope (Greve et al. 1998). All data reduction was done using the GILDAS[1] software package supported at IRAM.

3. Data

3.1. Molecular gas distribution

The HERA map of ^{12}CO 2−1 (Fig. 1) is the first CO map of M 51 encompassing the companion galaxy as well as the south-western arm out to a radius of ~12 kpc in a homogeneously sampled data set at linear scales of down to 450 pc.

The emission detected with the 30 m telescope traces the well known two-armed spiral pattern out to the companion galaxy NGC 5195, which shows up brightly in the north-east at ~10.5 kpc radial distance, and out to the south-western tip of the second arm at the opposite side of M 51. The outer parts of the two arms in the west and in the east appear more fragmented than the inner parts. The western arm especially is almost unresolved. Inter-arm emission is detected above the 3σ level out to radii of about 6 kpc. Several spoke-like structures connect the spiral arms radially.

To estimate the total H$_2$ column densities from the integrated CO 2−1 intensities, we assume a 2−1/1−0 intensity ratio of 0.8 as found by Garcia-Burillo et al. (1993b). Garcia-Burillo et al. (1993b) and Guélin et al. (1995) independently derived the CO-to-H$_2$ conversion factor X, for M 51 from CO 1−0 and dust continuum data. They find that it is a factor 4 smaller than the Milky Way value X_{MW} (Strong et al. 1988; Strong & Mattox 1996) and constant with radius. Similar X-factors for M 51 were found by Nakai & Kuno (1995), using CO data and visual extinctions towards H II regions, and by Adler et al. (1992) using BIMA CO 1−0 data assuming that the GMCs are in virial equilibrium.

For the total H$_2$ column density per beam in M 51, we use: $N(H_2) = 0.25 X_{MW} (1/0.8) \int T_{mb}(CO(2-1)) dv$ with $X_{MW} = 2.3 \times 10^{20}$ cm^{-2} (K km s^{-1})$^{-1}$.

The X-factor may be a function of the metallicity in spiral galaxies as has been suggested by several authors (e.g. Arimoto et al. 1996). However, other factors like the radiation field or

---

[1] http://www.iram.fr/IRAMFR/GILDAS
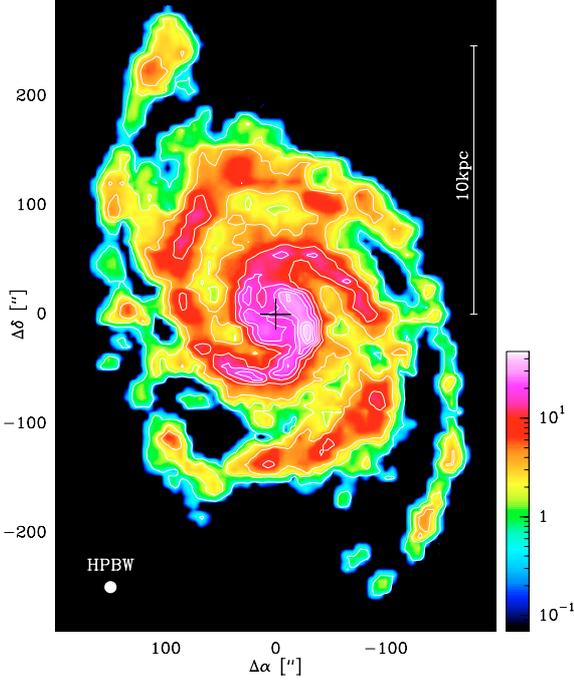
Fig. 1. Map of ^{12}CO 2−1 integrated intensities [K km s^{-1}] showing M 51, i.e. NGC 5194 and its companion galaxy NGC 5195 in the northeast. The image has a resolution of 11″ and is constructed from a masked moment calculation (Adler et al. 1992) to minimize the noise contribution from emission-free channels when integrating over the full kinematic extent of M 51, 350 km s^{-1} < v_{lsr} < 600 km s^{-1}. Color coded intensities are on a logarithmic scale. The cross marks the 0/0 center position at α = 13^{h}29^{m}52^s.7, δ = 47°11′43″ (eq.2000). The noise level is 1σ = 0.65 K km s^{-1}. Contours range in units of 1σ from 1, 3, 6, 16 to 56 in steps of 10. The peak intensity is 47.3 K km s^{-1}. All intensities are on the T_A^* scale.

Fig. 2. VLA map of integrated H I intensities [Jy/beam] at 13″ resolution (Rots et al. 1990) in colors. Contours show integrated ^{12}CO 2−1 intensities (cf. Fig. 1).
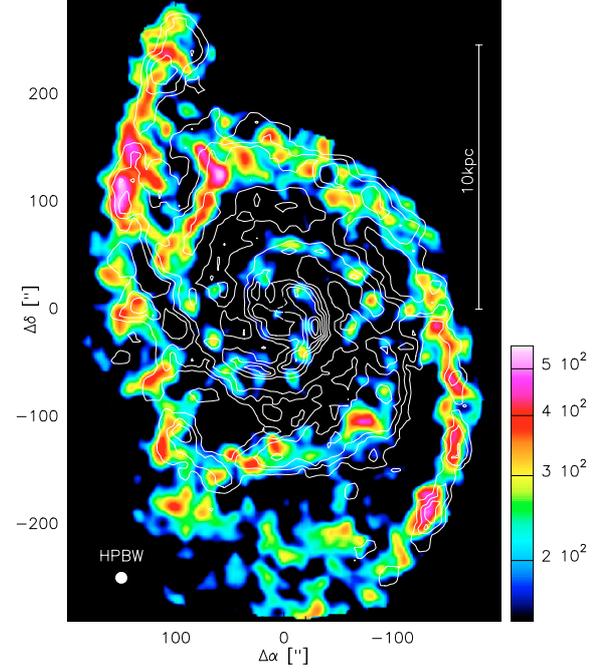
the cosmic-ray rate also have a strong impact on the CO-to-H$_2$ conversion factor (Bell et al. 2006). The metallicities of M 51 have been found to be slightly supersolar showing only a shallow drop with radius by only −0.02 dex kpc^{-1} (Bresolin et al. 2004): 12+log(O/H) = 8.72(±0.09)−0.28(±0.14)R/R_0 with R_0 = 5.4′. The almost constant metallicity appears to be consistent with a constant X-factor.

The 3σ limit with resolutions of 11″ and 5 km s^{-1} corresponds to a mass of 1.7×10^5 $M_\odot$. The spatial resolution of 450 pc does not allow to detect individual GMCs if their typical size is ~50 pc. The individual "clumps" delineating the spiral arms like beads on a string (Fig. 1) have been labeled giant molecular associations (GMAs). These may be bound clusters of GMCs as suggested by Rand & Kulkarni (1990) or random superpositions of molecular clouds and GMCs (Garcia-Burillo et al. 1993a).

The total mass of the molecular gas of M 51 derived from the CO 2−1 data set is $1.94 \times 10^9\,M_\odot$. This value agrees well with the total mass of $1.6 \times 10^9\,M_\odot$ derived by Helfer et al. (2003) from NRAO 12 m CO 1−0 data when using the same CO-to-H$_2$ conversion factor and distance.

3.2. H I and radio continuum

The large-scale distribution of the 21 cm line of atomic hydrogen in M 51 was analyzed by Rots et al. (1990) using the VLA. Note that the total flux is in reasonable agreement with single-dish observations (Rots 1980). The H I emission at 13″ resolution (Fig. 2) is weak in the inner region while the outer CO arms

are clearly delineated in H I. There is patchy H I emission in the south, near (0,−250″), where only very little CO is found. In the inner arms of M 51, inside the corotation radius of ~7.4 kpc (Garcia-Burillo et al. 1993a), H I and Hα emission (Rand & Kulkarni 1990; Tilanus & Allen 1991; Scoville et al. 2001) as well as young star cluster complexes (Bastian et al. 2005) are seen slightly towards the convex side, i.e. downstream relative to the CO emission, suggesting that they arise when GMCs are destroyed by short-lived OB stars. Figure 2 shows that the H I clouds tracing the south-western spiral arm, peak on the concave side of the CO arm. This is outside the corotation radius and thus again downstream, consistent with the above interpretation.

Figure 3 shows a map of the radio continuum (RC) at 20 cm (1.4 GHz) taken with the VLA at 15″ resolution (Patrikeev et al. 2006). Further below, we will use this map to derive the star formation rate per unit area. The radio continuum map shows strong emission in the inner arms, which slowly drops off towards the outer arms. There is patchy 20 cm emission in the south where there is H I but only very little CO. Again similar to H I, the 20 cm emission tracing the south-western spiral arm peaks on the concave, downstream side of the CO arm. The spiral arm near (−40″, 125″) shows an interesting discontinuity and local lack of radio continuum, H I, and CO emission. Patrikeev et al. (2006) discuss systematic offsets between the spiral arms traced by 6 cm radio continuum emission, ISOCAM data at 15 μm, and BIMA CO 1−0 emission over scales of several kpc.

4. Results

We investigate the correlation of H$_2$ and H I surface densities with star forming activity along radial averages, including the outskirts of the disk where H I dominates.

Various tracers of star formation such as Hα, UV, the far infrared continuum, and the radio continuum are frequently used. Hα emission is directly linked to OB associations but subject to
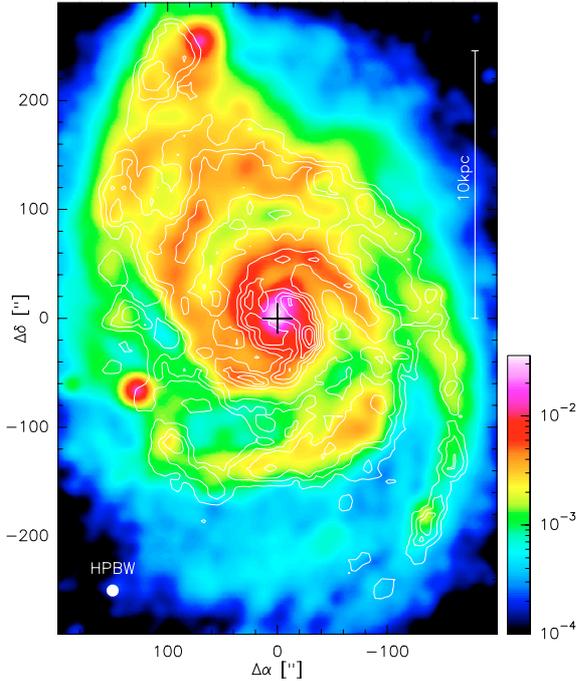
**Fig. 3.** Map of radio continuum intensities at 20 cm (VLA C+D, 15″ resolution) in units of Jy/beam (Patrikeev et al. 2006). Contours show integrated ^{12}CO 2−1 intensities (cf. Fig. 1).

Fig. 4. Radial distributions of surface densities of H_2, H I, the total gas, and the star formation rate per unit area in M 51. The lower box shows the ratios $\Sigma_{gas}/\Sigma_{SFR}$ and $\Sigma_{H_2}/\Sigma_{SFR}$.

extinction. See Bastian et al. (2005) for a recent study of the local star formation rate in M 51, derived from Hα images. Optically thin far-infrared (FIR) emission is usually taken as the most direct indicator of star formation. In a recent study, Calzetti et al. (2005) used MIPS/Spitzer 24 μm maps to study the star formation rate. Some questions remain however in regions of diffuse FIR emission from the atomic ISM. In such regions the dominant contribution to the FIR flux may be due to radiation heating of dust by the normal interstellar radiation field (Cox & Mezger 1989) and thus not trace star formation.

The radio continuum has widely been accepted as an alternative measure for star formation activity, a fact which is underlined by the very strong FIR/RC correlation in many different galaxies (see the review by Condon 1992). The FIR/RC correlation holds also on local scales of a few hundred parsecs comparable to the resolution of our data set. See Murphy et al. (2005) who recently studied this relation in M 51. Here, we use a new large scale 20 cm map of Patrikeev et al. (2006) at 15″ resolution and assume that the 20 cm radiation can be used as a direct indicator for the star formation rate. We use the FIR/RC correlation and a subsequent SFR/FIR conversion to derive the star formation rate. We then compare the star formation rate with the H_2 and H I surface densities in order to check for star formation thresholds. We further use the measured CO 2−1 line widths to study the gravitational stability of the gas disk.

4.1. Radial distribution of the gas

Total H_2 column densities are derived from the integrated CO 2−1 intensities as described in Sect. 3.1. We derive the face-on surface density via $\Sigma_{H_2} = 2\,m_H N(H_2)\cos i$ with the atomic hydrogen mass m_H and the inclination angle i of M 51 (Table 1). The total H I column density is derived assuming optically thin emission: $N(HI) = 1.82 \times 10^{18} \int T_{mb} dv/(K\,km\,s^{-1})\,cm^{-2}$. The
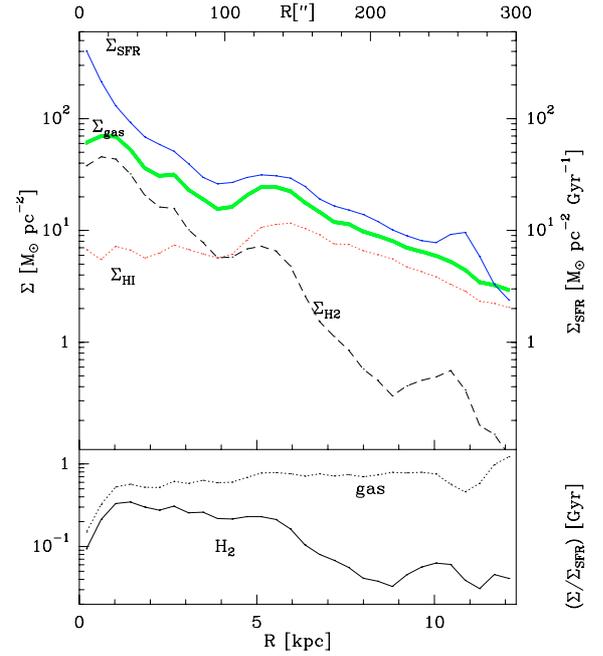
corresponding surface density is: $\Sigma_{HI} = m_H N(HI)\cos i$. The total molecular mass of M 51 is $1.94 \times 10^9\,M_\odot$ (Sect. 3.1) and the global ratio of H I over H_2 mass is 1.36. The molecular gas content of M 51 is similar to the total molecular mass of the Milky Way, $1.3 \times 10^9\,M_\odot$ (Misiriotis et al. 2006). However, the Milky Way has a larger fraction of H I mass. The ratio of H I over H_2 mass in the Milky Way is 6.3.

Figure 4 shows the radial profiles of the surface densities which were created by averaging in elliptical annuli spaced by 10″, including points of no detection, and centered at the 0/0 position. The annuli were assumed to be circular rings viewed at an inclination angle i and with a line of nodes rotated from north to east by the position angle PA as listed in Table 1.

Total gas surface densities are given by $\Sigma_{gas} = 1.36(\Sigma_{H_2} + \Sigma_{HI})$ which includes helium. The radially averaged Σ_{gas} drops by a factor of ∼20 from 70 $M_\odot$ pc^{-2} in the center to 3 $M_\odot$ pc^{-2} at radii of 12.2 kpc (300″) (Fig. 4).

Figure 5 shows the variation of Σ_{HI}/Σ_{H_2} with radius in M 51. Standard deviations of the mean Σ_{HI} and Σ_{H_2} are calculated from the rms values along the annular averages: $\sigma = $ rms $(N_{pix}/n_{beam})^{-0.5}$, following Wong & Blitz (2002) with the number of pixels per annulus N_{pix} and the number of pixels per beam n_{beam}. The fraction of atomic gas gradually increases with radius. In the inner regions of M 51, up to ∼6 kpc, the ratio of HI to H_2 surface density scales roughly with $R^{1.5}$. As the radial HI profile in M 51 is roughly constant, varying only by a factor of ∼5, the power-law dependence of the ratio of molecular and atomic gas is largely due to the decrease of the molecular gas surface density which drops by more than 2 orders of magnitude. The H I gas surface density starts to exceed the molecular surface density at radii greater than 4 kpc. The outer regions show deviate from any simple power-law. The peak Σ_{HI}/Σ_{H_2} fraction reaches values of 20 in the outer areas of our map.

We also plot the fraction of atomic gas for the seven spirals studied by Wong & Blitz (2002) and for M 33 studied by Heyer et al. (2004). In the center regions, the Σ_{HI}/Σ_{H_2} ratio of
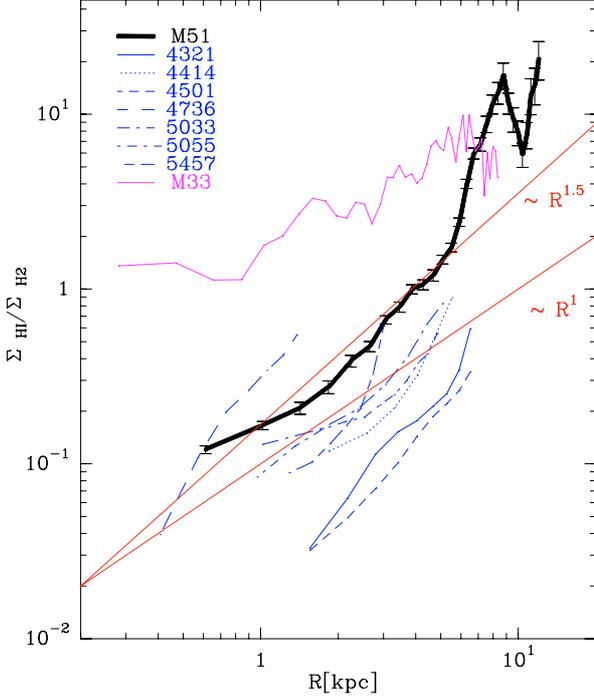
Fig. 5. Radial distribution of the ratio of atomic $\sum_{\mathrm{HI}}$ to molecular surface densities $\sum_{\mathrm{H_2}}$ for M 51 (thick line), the six spirals of the sample of Wong & Blitz (2002), and M 33 (Heyer et al. 2004). For comparison, we show two power-laws, one where the ratio scales with $R^{1.5}$ and one where it scales with R.

the nine galaxies varies strongly between 0.03 in NGC 4321 and slightly more than 1 in M 33. With the exception of M 33, the inner regions are clearly dominated by molecular material. For the galaxies of the Wong sample, the ratio scales roughly with $R^{1.5}$ for radii upto ~6 kpc. In M 33, the atomic gas dominates the total gas surface density for the entire disk, in strong contrast to the other 8 spirals (Fig. 5). The slope is much more shallow: the fraction of atomic gas scales with $R^{0.6}$ only (Heyer et al. 2004). At ~7 kpc, the fraction equals the fraction found at that distance in M 51.

Next, we compare the total gas surface densities with the star formation rate derived from the 20 cm radio continuum data.

4.2. Star formation rate and local Schmidt law

The radio continuum emission of the disk of M 51 reflects the spatial distribution of the current star formation rate. In normal galaxies, such as M 51, most of the radio continuum at 20 cm is non-thermal synchrotron emission (Condon 1992), radiated by cosmic rays interacting with the magnetic fields of the interstellar medium. The cosmic rays in turn are emitted by supernova remnants. The remaining radio continuum emission is free-free bremsstrahlung emission from thermal electrons in H II-regions. The radio continuum thus traces the current star formation rate of massive stars.

The observed optically thin radio continuum emission is known to be well correlated with FIR dust continuum emission in a large variety of sources, including normal disk galaxies. The tight correlation was confirmed by Helou et al. (1985) using IRAS data and is described by the parameter

$$q = \log\left(\frac{\mathrm{FIR}}{[3.75 \times 10^{12}\,\mathrm{W\,m^{-2}}]}\right) - \log\left(\frac{S_{20\,\mathrm{cm}}}{[\mathrm{Jy}]}\right). \qquad (1)$$

The parameter q was found to be 2.3 with a dispersion of ~0.2 dex in a wide variety of sources (Condon 1992). We used this relation to derive the FIR flux at 15″ resolution at each position in M 51. Murphy et al. (2005) have recently confirmed that this correlation holds for a map of M 51 at 70 μm using MIPS/Spitzer at 19″ resolution. In the disk, they find a median and scatter of $q_{70} = 1.94 \pm 0.19$. Note that the correlation is expected to break down at yet smaller scales of a few hundred parsecs around massive star-forming regions (Boulanger & Perault 1988).

The FIR intensity reflects the current star formation rate (see e.g. Yun et al. 2001), as young stars form deeply embedded in their parental molecular clouds, before dispersing their environment by forming H II regions and by supernovae explosions. Following the argument of Thronson & Telesco (1986), the FIR luminosity is proportional to the star formation rate:

$$L_{\mathrm{FIR}} = \mathrm{SFR}\, t_{\mathrm{FIR}}\, L/M \qquad (2)$$

where L/M is the luminosity-to-mass ratio of the young stellar clusters. Assuming a typical disruption time-scale of $t_{\mathrm{FIR}} = 2 \times 10^6$ yr and a Salpeter initial mass function (IMF), the current star formation rate is $SFR = 6.5 \times 10^{-10}\,(L_{\mathrm{FIR}}/L_\odot)\,M_\odot\,\mathrm{yr^{-1}}$. In summary, the star formation rate per unit area is related to the flux density at 20 cm via

$$\frac{\sum_{\mathrm{SFR}}}{[M_\odot\,\mathrm{pc^{-2}\,Gyr^{-1}}]} = 1.53 \times 10^5\,\frac{S_{20\,\mathrm{cm}}}{[\mathrm{Jy\,beam^{-1}}]}. \qquad (3)$$

The gas depletion or consumption time is defined as $\tau_{\mathrm{gas}} = \sum_{\mathrm{gas}} / \sum_{\mathrm{SFR}}$. This is the time which would be needed to convert the total gas content into stars assuming that the SFR is constant with time and that there is no gas infall or recycling via stellar winds. Note that the inverse of the gas depletion time is the star formation efficiency.

The global star formation rate of M 51 is 2.56 $M_\odot\,\mathrm{yr^{-1}}$ and the global gas depletion time 0.76 Gyr. The latter value corresponds to a global star formation efficiency (SFE) of 13% per 0.1 Gyr. Both values, the depletion time and the SFE, agree to within a factor of 2 with the values derived by Scoville et al. (2001) from Hubble Space Telescope (HST) Hα images and CO data. Misiriotis et al. (2006) have recently studied the distribution of the ISM in the Milky Way. They find a similar SFR of 2.7 $M_\odot\,\mathrm{yr^{-1}}$ but factor ~5 larger gas depletion time of 3.57 Gyr in the Milky Way. Typical normal spiral galaxies need less time than found in the Milky Way, but more time than found in M 51, to consume all the gas into stars. Kennicutt (1998) finds a median depletion time of 2.1 Gyr for his sample of 61 normal disk galaxies which shows variations between 0.2 Gyr in starburst galaxies like NGC 5169 and 12 Gyr in early-type spirals such as M 31.

The SFR peaks above 100 $M_\odot\,\mathrm{pc^{-2}\,Gyr^{-1}}$ in the center (Fig. 4), indicating a nuclear starburst, and drops radially to values of 3 $M_\odot\,\mathrm{pc^{-2}\,Gyr^{-1}}$ at 12 kpc distance. Note that the C2 cluster complex studied by Bastian et al. (2005) shows a local SFR of 2600 $M_\odot\,\mathrm{pc^{-2}\,Gyr^{-1}}$, while the other complexes studied by these authors show moderate local rates of ~60−70 $M_\odot\,\mathrm{pc^{-2}\,Gyr^{-1}}$. Regions of more than ~100 $M_\odot\,\mathrm{pc^{-2}\,Gyr^{-1}}$ (i.e. 0.1 $M_\odot\,\mathrm{kpc^{-2}\,yr^{-1}}$) are classified as starbursts (e.g. Kennicutt 1998). The center of M 51 harbours a Seyfert 2 AGN surrounded by a ~100 pc disk/torus (Kohno et al. 1996) of warm and dense gas (Matsushita et al. 1998, 2004).

Figure 4 shows the variation of the radially averaged star formation rate in comparison with the H I, H$_2$, and total gas surface densities in M 51. Ignoring the center, the radial drop of the star
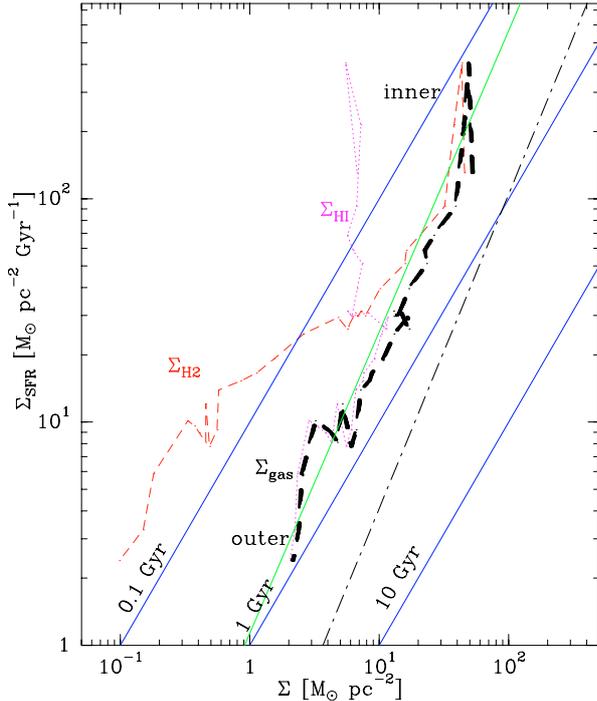
Fig. 6. Radially averaged star formation rate per unit area, Σ_{SFR}, versus surface densities of the total gas Σ_{gas}, and of H$_2$ and H I only. The solid green line is the local Schmidt-law found in M 51. The dashed-dotted black line is the global Schmidt-law found by Kennicutt (1998). Drawn blue lines represent lines of constant gas depletion time or star formation efficiency.

formation rate closely resembles the drop of the total gas surface density. Neither does the SFR show the rather flat distribution of the atomic gas nor the much steeper drop of the molecular gas. In contrast, we would have anticipated a good correlation of the star formation rate with the molecular gas since star formation is known to occur only in molecular clouds. Indeed, Heyer et al. (2004) find a strong correlation between the star formation rate and the molecular gas surface density in M 33. Similarly, Wong & Blitz (2002) report a much better correlation of Σ_{SFR} with Σ_{H2} than with Σ_{HI} in their sample of 6 molecule-rich spirals. However, Kennicutt (1998) who studied 88 galaxies and found that the disk-averaged SFR is much better correlated with the disk-averaged H I surface densities than with the H$_2$ surface densities. In M 51, H I is often found downstream of the CO arms indicating that the H I clouds are the remnants of GMCs photo-dissociated by young massive stars (Sect. 3.2). The star formation rate may thus regulate the surface density of the atomic gas and hence explain the observed correlation.

Figure 6 shows the variation of SFR in M 51 with gas surface densities together with lines of constant gas depletion time. The gas consumption time in M 51 varies between 0.1 Gyr in the center where the gas surface density and the SFR surface density are high and 1 Gyr at large radii where the gas surface density and SFR density are low (Figs. 4 and 6). In contrast, the Milky Way (Misiriotis et al. 2006) and the 6 CO-bright spiral galaxies studied by Wong & Blitz (2002) exhibit gas depletion times which are larger by a factor of about 10. They rise from ~1 Gyr in the centers to ~10 Gyr and slightly more in the outskirts.

Figure 6 also shows that the star formation rate is proportional to a power of the total gas surface density im M 51

$$\sum_{SFR} = A \sum_{gas}^{n} \tag{4}$$

i.e. follows a Schmidt-law (Schmidt 1959), with normalization $A = 1.1 \pm 0.5$ and the slope $n = 1.4 \pm 0.6$ where $\sum_{SFR}$ is in units of $M_\odot$ pc^{-2} Gyr^{-1} and $\sum_{gas}$ in units of $M_\odot$ pc^{-2}.

In Table 2, we compare the slope found in M 51 with the results obtained for other galaxies and the results from simulations. The slope found in M 51 agrees with the global Schmidt-law, seen in a study of disk-averaged $\sum_{gas}$ and $\sum_{SFR}$ of 61 normal and 36 starburst galaxies (Kennicutt 1998). Note however that the slope of the 61 normal galaxies is much less well-defined. Depending on the fitting method it varies between 1.3 and 2.5 (Kennicutt 1998).

In contrast, the observed slopes of *local* Schmidt laws, describing radial averages of $\sum_{gas}$ and $\sum_{SFR}$ in individual galaxies, do not in general agree with the global value, but vary strongly between 1.2 and 3.3. Wong & Blitz (2002) studied radial averages of $\sum_{gas}$ and $\sum_{SFR}$ in a sample of spiral galaxies and derive local Schmidt laws with slopes between 1.2 and 2.1, assuming that extinction depends on gas column density. Boissier et al. (2003) study 16 spiral galaxies to study the local star formation laws and find a slope of ~2. In a similar study, Heyer et al. (2004) shows that M 33 exhibits a significantly steeper slope of 3.3. Misiriotis et al. (2006) find a slope of 2.2 for the Milky Way.

4.3. Gravitational stability

Exceeding a critical gas density may lead to the formation of clouds and possibly stars. The critical density may in turn be determined by gravitation. Analogous to the well known Jeans stability criterion, the influence of differential rotation of a homogeneous, thin disk can be described by a dispersion relation for axially symetric disturbances (Kley 2004): $\sigma^2 = \kappa^2 + \sigma_{gas}^2 k^2 - 2\pi G \sum |k|$. Here, σ is the oscillation frequency, σ_{gas} the gas velocity dispersion, k the wavenumber, and κ the epicyclic frequency $\kappa^2 = \frac{2V}{R}\left(\frac{V}{R} + \frac{dV}{dR}\right)$. For a flat rotation curve, $\kappa^2 = 2\Omega^2$. The system becomes unstable when the Toomre parameter (Toomre 1964)

$$Q_{gas}(R) \equiv \frac{\Sigma_{crit}(R)}{\Sigma_{gas}(R)} = \frac{\kappa(R)\sigma_{gas}(R)}{\pi G \Sigma_{gas}(R)}, \tag{5}$$

describing the competition of pressure and rotation on the one side and gravitation on the other side, at a given radius, is less than 1, i.e. when the gas surface density exceeds the critical surface density.

In the following, we will assume that the disk of M 51 is almost unstable as predicted by disk models (e.g. Lin & Pringle 1987), i.e. $Q_{gas} = 1$, to calculate the critical gas velocity dispersion σ_{crit} necessary to stabilize the gas against gravitational collapse. We will then compare σ_{crit} with the observed velocity dispersion of the molecular gas, σ_{CO}, as function of the galactocentric radius.

4.3.1. Rotation curve

The rotation curve of M 51, needed to calculate the epicyclic frequency and the critical gas density (Eq. (5)), was derived by Garcia-Burillo et al. (1993b,a) from the CO 2−1 position-velocity diagram along the major axis of M 51, using the velocities at the peak intensities, and correcting for the inclination. The rotation curve (Fig. 7) rises steeply within 10″ of the center indicating the presence of a compact nuclear mass component in addition to the central bulge and then stays constant at ~200 km s^{-1} out to a radius of 10 kpc. We assume here that the rotation curve stays almost constant further out to at least 12 kpc, ignoring any

Table 2. Schmidt Law $\sum_{SFR} = A\sum_{gas}^{n}$ observed in M 51 and other galaxies in comparison with the Schmidt-Law derived from simulations. $\sum_{SFR}$ and A are in units of $M_\odot$ pc^{-2} Gyr^{-1} and $\sum_{gas}$ in units of $M_\odot$ pc^{-2}. The values of the sample of Wong & Blitz (2002) hold for an extinction correction that depends on the gas column density.

	A	n	Reference
Local Schmidt-laws:			
M 51	1.12 ± 0.50	1.35 ± 0.61	this paper
M 33	3.5 ± 66	3.3 ± 0.07	Heyer et al. (2004)
Milky Way		2.18 ± 0.20	Misiriotis et al. (2006)
7 CO-bright spiral galaxies		1.7 ± 0.3	Wong & Blitz (2002)
16 spiral galaxies		~2	Boissier et al. (2003)
simulations	0.25 ± 0.16	1.31 ± 0.15	Li et al. (2006)
Global Schmidt-laws:			
97 normal and starburst galaxies	0.25 ± 0.07	1.4 ± 0.15	Kennicutt (1998)
7 CO-bright spiral galaxies		1.7	Wong & Blitz (2002)
simulations	0.11 ± 0.04	1.56 ± 0.09	Li et al. (2006)
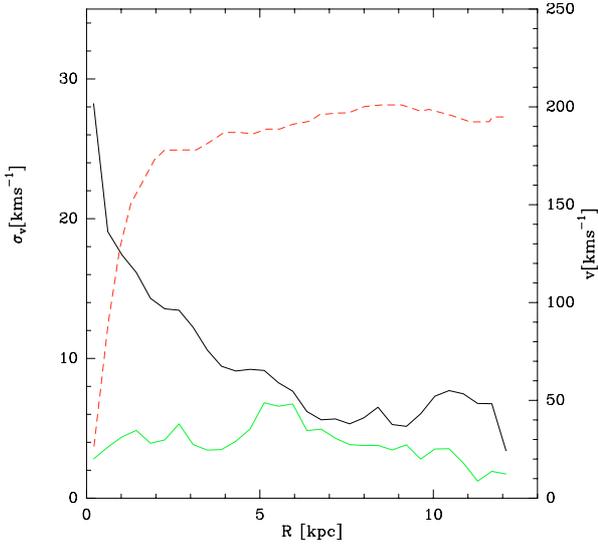
Fig. 7. *Left*: the black drawn line shows the ^{12}CO 2−1 gas dispersion σ_{CO} derived from the observed equivalent widths. Positions without detection of ^{12}CO are ignored. The green drawn line shows the gas dispersion σ_{crit}, assuming gravitational stability, i.e. $\Sigma_{crit} = \Sigma_{gas}$. *Right*: the dashed line gives the rotation curve derived by Garcia-Burillo et al. (1993a).

4.3.3. Observed velocity dispersion

The velocity dispersion of the molecular gas is estimated here from the equivalent ^{12}CO 2−1 line widths $\Delta v_{eq} = \int T \, dv / T_{pk}$ via $\sigma_{CO} = \Delta v_{eq}/(2\sqrt{2\ln 2})$. Figure 7 shows the radially averaged velocity dispersion σ_{CO}. It drops from ~28 km s^{-1} in the center to ~6 km s^{-1} at radii of 7 to 9 kpc. Further out, it rises again to values of ~8 km s^{-1}. The rise of the observed dispersion at radii of 10−13 kpc, is due to the increased line widths in the companion galaxy.

Similar vertical velocity dispersions are derived from H I observations of spiral galaxies. Typically, these vary radially from ~12−15 km s^{-1} in the central parts to ~4−6 km s^{-1} in the outer parts (see review of Dib et al. 2006).

The CO velocity dispersion observed in M 51 exceeds the critical dispersion at all radii. The ratio between the observed and the critical dispersions drop from a factor of ~5 to almost 1 for radii between 1 and 5 kpc. This may indicate that the gas is stabilized against collapse at all radii.

However, the observed gas dispersions are averages over the 450 pc beam and along the elliptical annuli, and are broadened relative to the intrinsic dispersions due to systematic motions which do not contribute necessarily to local support of the gas against gravity. Moreover, the influence of stars is neglected.

5. Discussion

5.1. Toomre stability

Several authors have argued that galactic disks are self-regulated through gravitational instabilities to have their Toomre Q parameter of the order of 1 (see e.g. Combes 2001). As soon as gas dissipation leads to $\Sigma_{gas} > \Sigma_{crit}$ at a given radius, the disk becomes gravitationally unstable, leading to density waves transferring angular momentum, causing dissipation and heating of the gas and thus an increase of the velocity dispersion, stabilizing the disk again. Models indeed indicate that the disk settles at the border of instability (Lin & Pringle 1987).

However, in general the velocity dispersion and surface density of stars may play an important role in the stability analysis. Bottema (1993) discuss the dispersion of stellar disks and the self-regulating mechanism that keeps Q near 1 over the entire disk of spiral galaxies. To take this into account, a total Q parameter has been used by e.g. Combes (2001): $Q_{tot}^{-1} = Q_{gas}^{-1} + Q_{star}^{-1}$. Neglecting stars is valid only when the gas surface density divided by the gas dispersion dominates all other Σ/σ terms.

effect of the companion galaxy. The definition of the rotation curve used here appears to be more appropriate for the face-on galaxy M 51 than the definition used by Sofue (1996) who derived the rotation curve from the terminal velocities at which the peak intensity has dropped to 20% of its value, which leads to very high velocities of up to 260 km s^{-1} at radii between 3 and 9 kpc.

4.3.2. Critical velocity dispersion

Figure 7 also shows the radially averaged critical velocity dispersion σ_{crit} derived from the gas surface density and the rotation curve, assuming $Q_{gas} = 1$ (Eq. (5)). The critical dispersion, necessary to stabilize the gas against gravitational collapse, lies between 1.7 and 6.8 km s^{-1}. The dispersion peaks near $R = 5.5$ kpc where the H$_2$ surface density is high (Fig. 4). It then declines slowly to ~2 km s^{-1} at $R = 12$ kpc.

Observationally, Q_{gas} has often been found to be larger than 1 by factors of a few. Kennicutt (1989) derived radial averages of the Toomre-parameter of a sample of 15 galaxies, assuming a constant velocity dispersion of 6 km s^{-1}, and found that star formation is restricted to regions where $Q_{gas} < 1.5$. A similar conclusion was drawn from a study of 32 nearby spiral galaxies by Martin & Kennicutt (2001) with few exceptions[2]. Similarly, Wong & Blitz (2002) also assume a constant velocity dispersion and find $\Sigma_{gas} \approx \Sigma_{crit}$ over a wider range of radii for some of their galaxies while others show deviations by factors of ~2.

While in the inner 4 kpc of M 51, the gas dispersion is large and Q_{gas} lies between 2 and 5, the stars may contribute here, and make the disk marginally stable. Streaming motions are a consequence of spiral waves and gravitational instabilities (Combes 2001). M 51 shows strong streaming motions of 60−150 km s^{-1} in the plane of the galaxy in the inner spiral arms as can be seen in the interferometric CO maps of Aalto et al. (1999). The broadening of the velocity dispersions due to streaming motions is naturally taken into account here. However, the observed dispersion is also broadened by the very steep, unresolved rotation curve in the center of M 51. A more careful stability analysis would need to correct the observed dispersions for rotation gradients, take into account the influence of stars, and study individual regions of M 51 at high spatial resolution.

5.2. The local Schmidt law and star formation efficiency

Recent smoothed particle hydrodynamics (SPH) simulations of gravitational instability of isolated disk galaxies comprising a dark matter halo, a disk of stars, and isothermal gas by Li et al. (2005, 2006) find a slope of 1.31 of the local Schmidt law (Table 2), close to the slope of the global Schmidt law, which is also reproduced, and close to the slope of 1.35 found in M 51. On the other hand, the slope of 1.3 is at the low-end of the local Schmidt law slopes observed so far.

We find a normalization factor A of the local Schmidt law in M 51 of 1.12 $M_\odot$ pc^{-2} Gyr^{-1} (Table 2), similar to A of gas-rich models in Li et al. (2006). This is a factor 5 larger than the average value of the Li et al. (2006) models. It is also a factor 5 larger than the normalization found in the large sample of Kennicutt (1998).

Interestingly, the normal galaxies of the Kennicutt (1998) sample show on average a factor ~3 longer gas consumption times than found in M 51. In Sect. 4.2 we also noticed that the Milky Way (Misiriotis et al. 2006) and the 6 CO-bright galaxies studied by Wong & Blitz (2002) exhibit consumption times which are larger than the consumption time found in M 51 by about one order of magnitude. Apparently, the star formation efficiency of M 51 is higher than in many other normal galaxies.

The reason may be the interaction of M 51 with its neighbouring galaxy NGC 5195, as has been proposed before as mentioned in the Introduction (e.g. Nikola et al. 2001; Howard & Byrd 1990; Toomre & Toomre 1972). This is supported by the recent simulations of Li et al. (2004) which show that interaction and merging can lead to instable disks and strong starbursts.

---

[2] Both, Kennicutt (1989) and Martin & Kennicutt (2001) included M 51 in their sample, using FCRAO 50″ CO 1−0 data combined with Hα data. However, the Toomre parameter and its variation with radius in M 51 are not explicitly discussed.

6. Summary

We mapped completely the interacting spiral galaxy M 51 in the ^{12}CO 2−1 line using HERA at the IRAM-30 m telescope. The map includes the companion galaxy as well as the south-western arm out to radii of 12 kpc at linear resolutions of 450 pc (11″). These data were combined with maps of H I and the radio continuum at 20 cm at similar resolutions to study radially averaged surface densities. The star formation rate per unit area was estimated from the radio continuum, allowing to study star formation laws like the Schmidt law. The critical density for gravitational instability was compared with the total gas surface density along the radial averages. In detail, we obtain the following results:

− Global properties: The total H$_2$ mass of M 51 is 1.94×10^9 $M_\odot$ and the global H I/H$_2$ mass ratio is 1.36. The global star formation rate is 2.56 $M_\odot$ yr^{-1} and the global gas depletion time is 0.8 Gyr.
− The total gas surface density drops from ~70 $M_\odot$ pc^{-2} in the center to ~3 $M_\odot$ pc^{-2} at radii of 12 kpc. The ratio of atomic to molecular gas surface density rises from 0.1 in the center to 20 in the outer regions. It is 1 at ~4 kpc. Up to ~6 kpc the ratio follows a simple power law of $R^{1.5}$ similar to that found in other spirals. At larger radii, the simple power law relation breaks down.
− The gas depletion times in M 51, vary between 0.1 and 1 Gyr, and are shorter than in many other non-interacting normal galaxies. Simulations indeed show that interaction can lead to high star formation efficiencies.
− The star formation rate per unit area drops from ~400 $M_\odot$ pc^{-2} Gyr^{-1} in the starburst center to ~2 $M_\odot$ pc^{-2} Gyr^{-1} in the outskirts. It is much better correlated with the total gas surface density than with the surface densities of the molecular or atomic gas. The correlation follows a Schmidt law $\Sigma_{SFR} \propto \Sigma_{gas}^n$ with an index of $n = 1.4 \pm 0.6$. Only few studies of local Schmidt laws exist to date. The slopes of local Schmidt laws observed in other spirals vary strongly between 1.2 and 3.3. The slope of 1.4 agrees with recent SPH simulations of isolated disk galaxies Li et al. (2005).
− The radially averaged dispersion of the observed ^{12}CO 2−1 lines varies between 28 km s^{-1} in the center and ~6 km s^{-1} in the outskirts.
− We investigated the gravitational stability using the Toomre criterion. The critical gas velocity dispersions needed to stabilize the gas against gravitational collapse in the differentially rotating disk of M 51, vary with radius between 1.7 and 6.8 km s^{-1}. Observed radially averaged dispersions derived from the CO data exceed the critical dispersions by factors Q_{gas} of 1 to 5. Unresolved gradients of the rotation curve lead to an overestimate of the intrinsic velocity dispersion. The gravitational potential of stars not considered here, may lead to a marginally stable disk.

In a forthcoming paper we will discuss the distribution of molecular gas, local Schmidt laws, and local critical gas surface densities, discerning the conditions in different parts of M 51, i.e. the arm, interarm, and central regions. We will also study in more detail the spatial and kinematic distribution of atomic and molecular clouds, especially in the outer spiral arms.

References

Aalto, S., Huettemeister, S., Scoville, N. Z., & Thaddeus, P. 1999, ApJ, 522, 165

Adler, D. S., Lo, K. Y., Wright, M. C. H., et al. 1992, ApJ, 392, 497

Arimoto, N., Sofue, Y., & Tsujimoto, T. 1996, PASJ, 48, 275

Bastian, N., Gieles, M., Efremov, Y. N., & Lamers, H. J. G. L. M. 2005, A&A, 443, 79

Bell, T. A., Roueff, E., Viti, S., & Williams, D. A. 2006, MNRAS, 371, 1865

Boissier, S., Prantzos, N., Boselli, A., & Gavazzi, G. 2003, MNRAS, 346, 1215

Bottema, R. 1993, A&A, 275, 16

Boulanger, F., & Perault, M. 1988, ApJ, 330, 964

Bresolin, F., Garnett, D. R., & Kennicutt, R. C. 2004, ApJ, 615, 228

Calzetti, D., Kennicutt, R. C., Bianchi, L., et al. 2005, ApJ, 633, 871

Combes, F. 2001, in The Central Kiloparsec of Starbursts and AGN: The La Palma Connection, ed. J. H. Knapen, J. E. Beckman, I. Shlosman, & T. J. Mahoney, ASP Conf. Ser., 249, 475

Condon, J. J. 1992, ARA&A, 30, 575

Cox, P., & Mezger, P. G. 1989, A&ARv, 1, 49

Daigle, O., Carignan, C., Amram, P., et al. 2006, MNRAS, 367, 469

de Vaucouleurs, G., de Vaucouleurs, A., Corwin, H. J., et al. 1991, Third reference catalogue of bright galaxies (New York: Springer-Verlag)

Dib, S., Bell, E., & Burkert, A. 2006, ApJ, 638, 797

Elmegreen, B. G. 1994, ApJ, 425, L73

Feldmeier, J. J., Ciardullo, R., & Jacoby, G. H. 1997, ApJ, 479, 231

Garcia-Burillo, S., Combes, F., & Gerin, M. 1993a, A&A, 274, 148

Garcia-Burillo, S., Guelin, M., & Cernicharo, J. 1993b, A&A, 274, 123

Gerin, M., & Phillips, T. 2000, ApJ, 537, 644

Greve, A., Kramer, C., & Wild, W. 1998, A&AS, 133, 271

Guélin, M., Zylka, R., Mezger, P. G., Haslam, C. G. T., & Kreysa, E. 1995, A&A, 298, L29

Helfer, T. T., Thornley, M. D., Regan, M. W., et al. 2003, ApJS, 145, 259

Helou, G., Soifer, B. T., & Rowan-Robinson, M. 1985, ApJ, 298, L7

Heyer, M. H., Corbelli, E., Schneider, S. E., & Young, J. S. 2004, ApJ, 602, 723

Howard, S., & Byrd, G. G. 1990, AJ, 99, 1798

Israel, F. P., & Baas, F. 2002, A&A, 383, 82

Israel, F. P., Tilanus, R. P. J., & Baas, F. 2006, A&A, 445, 907

Kennicutt, R. C. 1989, ApJ, 344, 685

Kennicutt, R. C. 1998, ApJ, 498, 541

Kley, P. 2004, Theoretische Astrophysik, Wintersemester 2004/05 (Universitaet Tuebingen)

Kohno, K., Kawabe, R., Tosaki, T., & Okumura, S. 1996, ApJ, 461, L29

Kramer, C., Mookerjea, B., Bayet, E., et al. 2005, A&A, 441, 961

Kuno, N., & Nakai, N. 1997, PASJ, 49, 279

Kuno, N., Nakai, N., Handa, T., & Sofue, Y. 1995, PASJ, 47, 745

Lin, D. N. C., & Pringle, J. E. 1987, MNRAS, 225, 607

Li, Y., Mac Low, M.-M., & Klessen, R. S. 2004, ApJ, 614, L29

Li, Y., Mac Low, M.-M., & Klessen, R. S. 2005, ApJ, 620, L19

Li, Y., Mac Low, M.-M., & Klessen, R. S. 2006, ApJ, 639, 879

Lord, S., & Young, J. 1990, ApJ, 356, 135

Martin, C. L., & Kennicutt, R. C. 2001, ApJ, 555, 301

Matsushita, S., Kohno, K., Vila-Vilaro, B., Tosaki, T., & Kawabe, R. 1998, ApJ, 495, 267

Matsushita, S., Sakamoto, K., Kuo, C.-Y., et al. 2004, ApJ, 616, L55

Meijerink, R., Tilanus, R. P. J., Dullemond, C. P., Israel, F. P., & van der Werf, P. P. 2005, A&A, 430, 427

Misiriotis, A., Xilouris, E. M., Papamastorakis, J., Boumis, P., & Goudis, C. D. 2006, in press

Murphy, E. J., Armus, L., Helou, G., Braun, R., & the SINGS team. 2005, in The Spitzer Space Telescope: New Views of the Cosmos, ed. L. Armus & et al. (ASP Conference Series)

Nakai, N., & Kuno, N. 1995, PASJ, 47, 761

Nakai, N., Kuno, N., Handa, T., & Y. Sofue, Y. 1994, PASJ, 46, 527

Nikola, T., Geis, N., Herrmann, F., et al. 2001, ApJ, 561, 203

Patrikeev, I., Fletcher, A., Stepanov, R., et al. 2006, in press

Rand, R. J., & Kulkarni, S. R. 1990, ApJ, 349, L43

Rots, A. 1980, A&AS, 41, 189

Rots, A., Crane, P., Bosma, A., Athanassoula, E., & van der Hulst, J. 1990, AJ, 100, 387

Rydbeck, G., Thomasson, M., Aalto, S., Johansson, L., & Hüttemeister, S. 2004, in The Neutral ISM in Starburst Galaxies, ed. S. Aalto, S. Huttemeister, & A. Pedlar, ASP Conf. Ser., 320, 152

Schinnerer, E., Weiß, A., Aalto, S., & Scoville, N. Z. 2004, in The Dense Interstellar Medium in Galaxies, ed. S. Pfalzner, C. Kramer, C. Straubmeier, & A. Heithausen, 117

Schmidt, M. 1959, ApJ, 129, 243

Schuster, K.-F., Boucher, C., Brunswig, W., et al. 2004, A&A, 423, 1171

Scoville, N., & Young, J. S. 1983, ApJ, 265, 148

Scoville, N. Z., Polletta, M., Ewald, S., et al. 2001, AJ, 122, 3017

Sofue, Y. 1996, ApJ, 458, 120

Strong, A. W., & Mattox, J. R. 1996, A&A, 308, L21

Strong, A. W., Bloemen, J. B. G. M., Dame, T. M., et al. 1988, A&A, 207, 1

Takats, K., & Vinko, J. 2006, MNRAS, in press

Thronson, H. A., & Telesco, C. M. 1986, ApJ, 311, 98

Tilanus, R. P. J., & Allen, R. J. 1991, A&A, 244, 8

Toomre, A. 1964, ApJ, 139, 1217

Toomre, A., & Toomre, J. 1972, ApJ, 178, 623

Tully, R. B. 1974a, ApJS, 27, 437

Tully, R. B. 1974b, ApJS, 27, 449

Wong, T., & Blitz, L. 2002, ApJ, 569, 157

Yun, M. S., Reddy, N. A., & Condon, J. J. 2001, ApJ, 554, 803